A Cost Function-Free Modulated Model Predictive Control Technique for PMSM by the Geometric Derivations

Zhen Huang, Qiang Wei, Hongwei Tao, Tingfeng Wu, Yonghong Xia, and Marco Rivera

***Abstract*—Modulated model predictive control (MMPC) technique has shown promise in high-performance PMSM control. However, in the implementation of MMPC technology, the vector duty cycle calculation is completely dependent on the cost function (CF). Unfortunately, under the three common CFs, the calculated duty cycle has a certain error. To address this issue, a CF-free MMPC method based on geometric derivation is proposed. This method uses the relationship between vector projection and geometry to calculate the duty cycle accurately, which greatly improves the steady-state performance of the system. In addition, the inaccuracy of the duty cycle calculation of the MMPC method under three CFs is evaluated by the visual analysis method. Finally, the hardware-in-the-loop and the experiment on 1500rpm permanent magnet synchronous motor (PMSM) driver are carried out to verify the superiority of the proposed method.**

***Index Terms*—cost function free, duty cycle, modulated model predictive control, vector projection, visual evaluation**

I. INTRODUCTION

Due to the advantages of high power density, low maintenance cost, and excellent control performance, permanent magnet synchronous motors (PMSM) have been widely used in transportation, industrial transmission, and other fields [1]-[3]. With the continuous improvement of motor reliability requirements, traditional field-oriented control (FOC) cannot meet complex operating conditions [4]. Its PI regulator lacks nonlinear control capability, which may lead to performance degradation under system disturbance. In addition, the calculation of appropriate regulatory parameters becomes increasingly complex [5]. Therefore, in recent years, an effective and advanced control strategy model predictive control (MPC) has been considered to overcome the shortcomings of the FOC scheme [6]-[8].

MPC is a control method that uses a system model to predict future behavior in a certain prediction time domain and determines the control action by minimizing the error between the predicted value and the reference value [9]. Its advantage is that the algorithm itself is consistent with the discrete characteristics of a two-level voltage source inverter. The MPC method not only reduces the dependence on the PI regulator but also provides fast and effective control results in nonlinear systems [10]. However, an inherent limitation of the MPC approach is that only one voltage vector is used in one control cycle, resulting in a large torque ripple and variable switching frequency [11], [12].

To address this challenge, a modulated model predictive control (MMPC) strategy using multiple voltage vectors in each control cycle has been proposed and investigated [13]-[17]. By using three vectors in the same sector in one control period, this method not only achieves a fixed switching frequency but also greatly reduces the current ripple. As a result, the MMPC approach has gained widespread adoption in various applications such as motor drives [15], [16], multilevel inverters [17], [18], three-phase active rectifiers [19], [20], grid-connected power converters [21]-[23], etc.

However, the duty cycle calculation of MMPC schemes is always a difficult problem [24], [25]. The duty cycle obtained by minimizing the weighted error in the traditional MMPC method is numerically inversely related to the cost function (CF) [13]. Therefore, the accuracy of duty cycle calculation is significantly affected by the setting of the CF. At present, the three commonly used CFs are the Manhattan norm [14], the Euclidean norm [26], and the Euclidean norm square [16]. Unfortunately, there are some errors in the calculated duty cycle under these three CFs. Applying an incorrect duty cycle to the inverter will inevitably bring bad effects on the steady-state performance of the motor control.

In order to reduce the influence of the CF on the duty cycle calculation, some improved MMPC using such as the dead-beat principle [27], [28] and virtual vector technology [21], [25]have been proposed. The calculation of the duty cycle by these methods is not only dependent on the CF but also on theoretical approximation or iterative approximation. Although the duty cycle can be calculated further accurately, the computational complexity of the algorithm is greatly increased [16], which is different from the fast control theory of the MPC method. Therefore, a method to accurately calculate the duty cycle without sacrificing computing speed is urgently needed.

To solve the problem of duty cycle calculation, a CF-free MMPC method based on geometric derivation is proposed in this paper. This method uses the concept of vector projection to calculate the duty cycle accurately. Vector projection is calculated by the inner product of vectors; thus, the computational complexity is not increased. Compared with the traditional MMPC method, this method completely eliminates the CF and improves the accuracy of duty cycle calculation. Under the effect of this method, the accurate calculation of the duty cycle makes the steady-state performance of the system significantly improved. In addition, in order to illustrate the effect of CF on the duty cycle intuitively, three common CFs are analyzed by the visual analysis method in this paper. The proposed method is also theoretically verified by the same method.

This paper is organized as follows: Section II introduces the

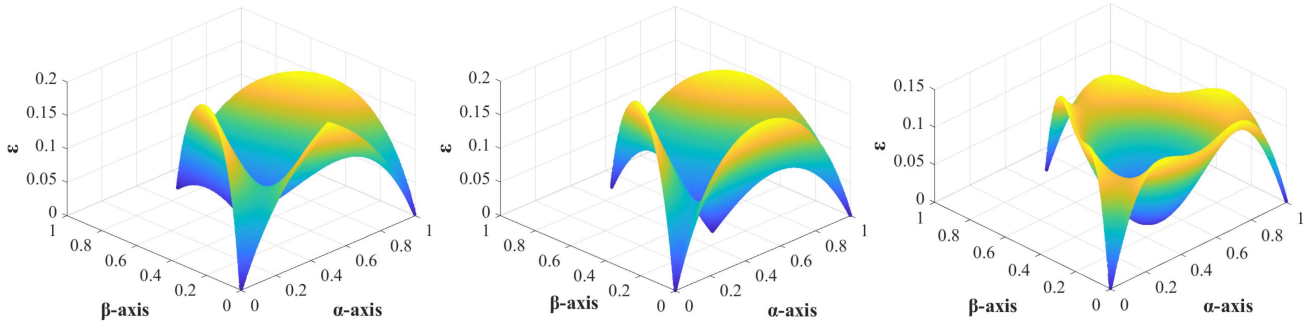

(a) 3-D of g_m (b) 3-D of g_e (c) 3-D of g_{es}

Fig. 1. Visualization error ε analysis under three CFs.

mathematical model of PMSM and the principles of MMPC, discussing the limitations of conventional MMPC approaches. Then, Section III provides a detailed introduction to the steps of the MMPC method proposed in this paper. Subsequently, the proposed method is verified by hardware-in-the-loop results in Section IV, and by experiments in Section V. Conclusions are drawn in Section VI.

II. Review of MMPC Method

A. Mathematical Model of PMSM

In the α-β coordinate system, the mathematical model of the three-phase PMSM based on forward Euler discretization is detailed as follows:

$$\begin{aligned} u_{\alpha ref}(k+1) &= Ri_{\alpha}(k) + L(i_{\alpha ref} - i_{\alpha}(k))/T_s - \omega_e \psi_f \sin\theta \\ u_{\beta ref}(k+1) &= Ri_{\beta}(k) + L(i_{\beta ref} - i_{\beta}(k))/T_s + \omega_e \psi_f \cos\theta \end{aligned} \quad (1)$$

where $u_{\alpha ref}(k+1)$ and $u_{\beta ref}(k+1)$ represent the predicted values of the α-axis and β-axis reference voltages at the next sampling instant, respectively. $i_{\alpha ref}$ and $i_{\beta ref}$ represent the reference values of the α-axis and β-axis currents. $i_{\alpha}(k)$ and $i_{\beta}(k)$ represent the measured values of the α-axis and β-axis currents at the current instant. T_s is the sampling period.

B. Principle of MMPC Method

In the traditional MMPC method, the CF is calculated for each of the seven vectors $V_i \in V_s = \{V_0, \ldots, V_6\}$. The optimization problem is to find the switching state corresponding to the minimum CF. Three kinds of CFs are usually selected for optimization, namely Manhattan norm $g_m(i)$, Euclidean norm $g_e(i)$, and Euclidean norm square $g_{es}(i)$

$$g_m(i) = \left|u_{\alpha ref} - u_{\alpha i}\right| + \left|u_{\beta ref} - u_{\beta i}\right| \quad (2)$$

$$g_e(i) = \left(\left(u_{\alpha ref} - u_{\alpha i}\right)^2 + \left(u_{\beta ref} - u_{\beta i}\right)^2\right)^{1/2} \quad (3)$$

$$g_{es}(i) = \left(u_{\alpha ref} - u_{\alpha i}\right)^2 + \left(u_{\beta ref} - u_{\beta i}\right)^2 \quad (4)$$

As for a two-level three-phase converter, enumerating the CFs of one zero vector and two adjacent active vectors in each sector. The derivation of the duty cycles for these three vectors is simplified as follows:

$$\begin{aligned} d_0 &= g_1 g_2 / (g_1 g_2 + g_1 g_0 + g_2 g_0) \\ d_1 &= g_0 g_2 / (g_1 g_2 + g_1 g_0 + g_2 g_0) \\ d_2 &= g_1 g_0 / (g_1 g_2 + g_1 g_0 + g_2 g_0) \end{aligned} \quad (5)$$

where d_0, d_1, and d_2 are the duty cycle for zero vector and two active vectors.

C. Drawbacks of the Conventional MMPC

For the synthetic voltage vector V'_{ref} output by the traditional MMPC method, there is actually a certain error with the input reference voltage. The error is due to the inaccuracy of the duty cycle calculation. In order to illustrate the inaccuracy of the duty cycle calculation of the traditional MMPC method, a visual analysis method is used to draw 3-D charts of ε, and the defects in the duty cycle calculation of the traditional MMPC method are vividly displayed. Where:

$$V'_{ref} = d_1 V_1 + d_2 V_2 \quad (6)$$

$$\varepsilon = \left|V_{ref} - V'_{ref}\right| \quad (7)$$

In addition, in the two-level voltage source inverter topology, the six sectors have similar properties due to symmetry; Therefore, this article only takes the first sector as an example.

Fig. 1 shows the error between the resultant voltage vector calculated by three different CFs and the actual reference voltage vector when the reference vector is located at any point in the first sector. From the 3-D (a) to (c), it can be observed that under the three CFs, the error of duty cycle calculation is zero only in a few regions, while there is a large error in most regions, especially at the edge.

It is worth noting that the MMPC method uses the square of the European norm as the CF has the least error of zero in the whole sector. However, none of the MMPC methods under the three CFs can guarantee zero error in the whole sector. These errors may accumulate when the system is working, resulting in the deterioration of the steady-state performance of the system and irreversible effects.

III. Proposed MMPC Method

According to the analysis in Section II.C, it can be concluded that the traditional MMPC method, using three CFs, has a large duty cycle calculation error. Therefore, a new CF-free-based MMPC method is proposed, and the concrete steps are

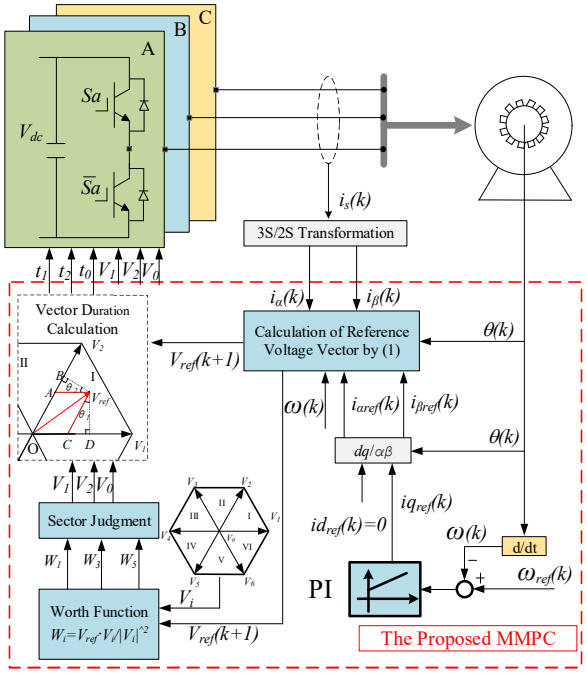

Fig. 2. The schematic of the proposed MMPC method.

discussed in this section.

A. Structure Diagram of the Proposed MMPC Technique

Fig. 2 shows the complete schematic diagram of the proposed MMPC method for PMSM with CF-free and accurate vector duty cycle calculation. The reference current of the α-β axis is generated by dq-$\alpha\beta$ variation, and then the reference voltage is predicted by a mathematical model of PMSM. Through the judgment of the worth function (WF), the sector is determined, which in turn simplifies the selection of the optimal vector (see Section III.B). A calculation strategy using WF and geometric relationship is proposed to determine the optimal duty cycle (see Section III.C). Finally, the selected vector combination and the corresponding duration are applied to the inverter to drive the motor.

B. Vector Selection

For intuitive selection, the entire α, β plane is divided into six sectors, as shown in Fig. 3. The arrow points in the positive direction. WF is defined as the vector projection ratio. In order to reduce the computational burden of the digital processor, WF

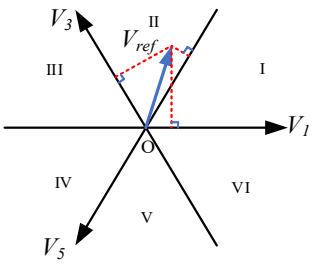

Fig. 3. The schematic of vector selection.

TABLE I

RELATIONSHIP BETWEEN THE WF AND SELECTED VECTORS

Judgment conditions	The selected valid vector	Sector
$W_1>W_3>W_5$	V_1, V_2	I
$W_3>W_1>W_5$	V_2, V_3	II
$W_3>W_5>W_1$	V_3 V_4	III
$W_5>W_3>W_1$	V_4, V_5	IV
$W_5>W_1>W_3$	V_5, V_6	V
$W_1>W_5>W_3$	V_6, V_1	VI

is calculated from the inner product of the vector, and the specific expression is shown in (8).

$$W_i = \frac{V_{ref}^{\alpha}V_i^{\alpha} + V_{ref}^{\beta}V_i^{\beta}}{V_i^{\alpha}V_i^{\alpha} + V_i^{\beta}V_i^{\beta}} \tag{8}$$

Where i is the ordinal number of the valid vector. W_i is the WF of the i_{th} vector.

Assuming the reference vector is in the second sector, the relative order of the WF for V_1, V_3, and V_5 is $W_3>W_1>W_5$. Similarly, the relative order of the WF for the reference vector in other sectors can be determined. Therefore, it is only necessary to compute W_1, W_3, and W_5 and compare their magnitudes to determine the sector in which the reference vector is located and, consequently, select the corresponding vector. The specific sector correspondence and the selected active vector are shown in Table I.

C. Vector Duty Cycle Calculation

After the optimal vector is determined, the concrete steps of calculating duty cycle through the geometrically derived CF-free-based MMPC method are as follows. Taking the reference vector in the first sector as an example, as shown in Fig. 4. Then d_1, d_2, W_1, and W_2 are respectively

$$d_1 = \frac{|OC|}{|V_1|}, \quad d_2 = \frac{|OA|}{|V_2|} \tag{9}$$

$$W_1 = \frac{|OD|}{|V_1|}, \quad W_2 = \frac{|OB|}{|V_2|} \tag{10}$$

It can be obtained by the principle of a two-level inverter:

$$|V_i| = \frac{2}{3}V_{dc} \tag{11}$$

where d_1, d_2 indicates the duty cycle of V_1, V_2; V_{dc} is DC-link voltage. After that, by the geometric relationships: both θ_1 and θ_2 are equal to 30°. Therefore:

$$|AB| = \frac{1}{2}|A\_V_{ref}| = \frac{1}{2}|OC| \tag{12}$$

$$|CD| = \frac{1}{2}|C\_V_{ref}| = \frac{1}{2}|OA| \tag{13}$$

Thus:

$$\frac{1}{2}|OC| + |OA| = |OB| \tag{14}$$

$$\frac{1}{2}|OA| + |OC| = |OD| \tag{15}$$

Dividing the left and right sides of (14) and (15) by $2/3V_{dc}$

$$\frac{1}{2}\frac{|OC|}{2/3V_{dc}} + \frac{|OA|}{2/3V_{dc}} = \frac{|OB|}{2/3V_{dc}} \tag{16}$$

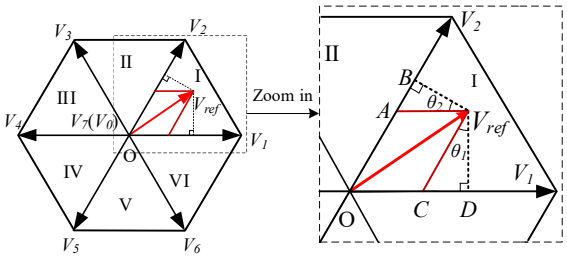

Fig. 4. Vector action time calculation schematic.

$$\frac{1}{2}\frac{|OA|}{2/3V_{dc}}+\frac{|OC|}{2/3V_{dc}}=\frac{|OD|}{2/3V_{dc}} \tag{17}$$

That is:

$$\frac{1}{2}d_1+d_2=W_2 \tag{18}$$

$$d_1+\frac{1}{2}d_2=W_1 \tag{19}$$

With (18) and (19), d_1 and d_2 can be easily found, i.e.,

$$d_1=\frac{4W_1-2W_2}{3} \tag{20}$$

$$d_2=\frac{4W_2-2W_1}{3} \tag{21}$$

When $d_1+d_2<1$:

$$t_1=d_1T_s,\ t_2=d_2T_s,\ t_0=T_s-t_1-t_2 \tag{22}$$

When $d_1+d_2>1$:

$$t_1=\frac{d_1T_s}{d_1+d_2},\ t_2=\frac{d_2T_s}{d_1+d_2},\ t_0=0 \tag{23}$$

D. Flowchart of the Proposed MMPC Technique

The flowchart of the proposed CF-free-based MMPC method is shown in Fig. 5. To begin with, the proposed method first obtains the α-β-axis current by measurement. Based on the principle of dead-beat, the reference value of current is used as the predicted value of current at the next time, and the reference voltage at the next time is obtained. Then the selected vector is determined by projection calculation combined with Table I, and the duration of each vector is calculated by (20)-(23).

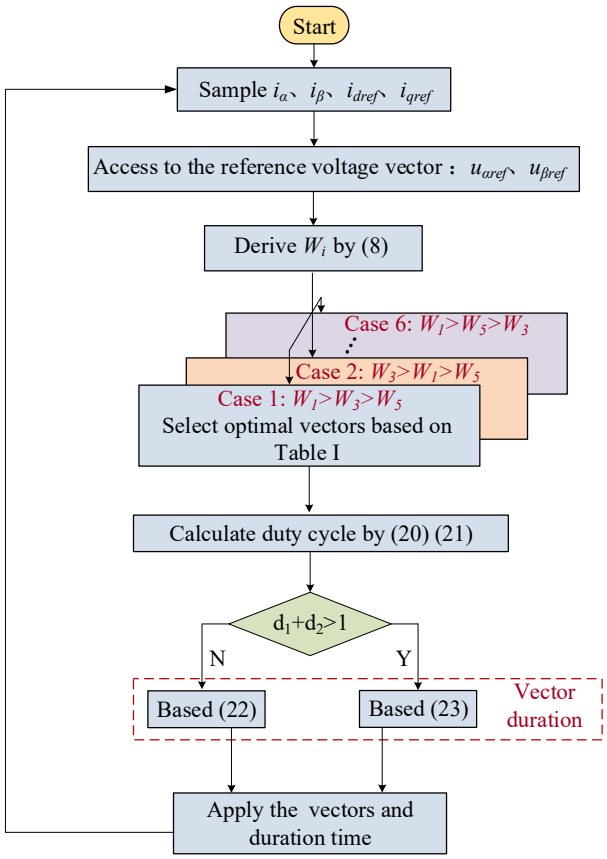

Fig. 5. The flowchart of the proposed MMPC method.

Finally, within a cycle, the switching state of the selected vector corresponds to the inverter applied during the corresponding period.

E. Effectiveness Evaluation

In this section, the effectiveness of the proposed MMPC strategy is demonstrated visually. As shown in Fig. 6, when the reference vector is located at any point in Sector I, the difference between the vector synthesis error of the proposed method and the traditional MMPC method is shown by 3-D graphs.

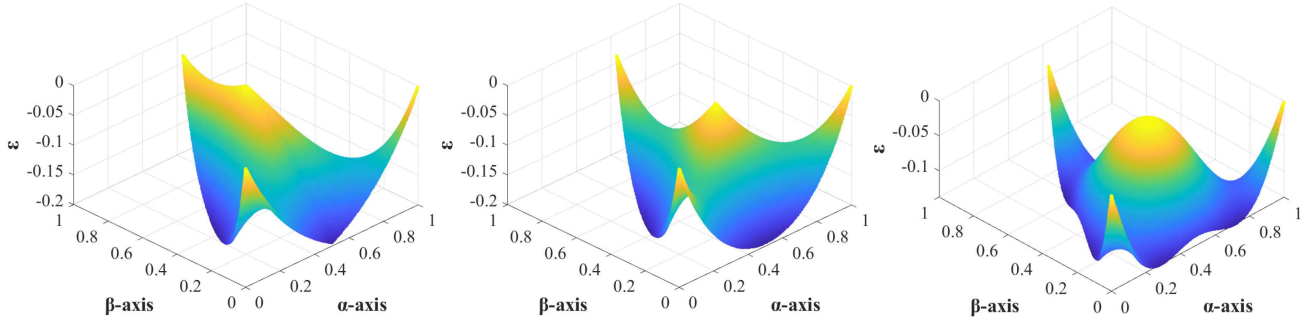

(a) 3-D of g_m (b) 3-D of g_e (c) 3-D of g_{es}

Fig. 6. Visual difference analysis of the vector synthesis error of the proposed method and the traditional MMPC method with three CFs.

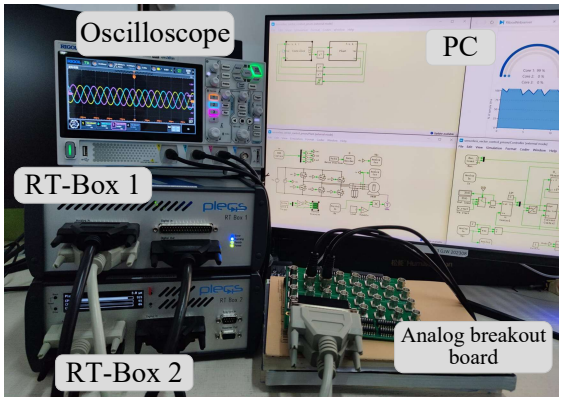

Fig. 7. Hardware-in-the-loop platform.

By looking at Fig. 6, it is clear that the difference is less than or equal to zero across the entire sector. This further emphasizes that over the whole sector, the duty cycle calculation accuracy of the proposed method is superior to that of the traditional MMPC algorithm, regardless of which of the three CFs is used in the traditional MMPC algorithm.

IV. Hardware-in-the-loop Results

A. Rig set-up

In this section, the proposed MMPC method is validated by real-time hardware-in-the-loop (HIL). This allows the real-time validity of the proposed CF-free MMPC method to be evaluated. Fig. 7 illustrates the utilization of an RT-Box to simulate the PMSM Drives model, capturing the switching behavior of PMSM Drives. A second RT-Box is employed to receive signals from the simulated analog-to-digital channel feedback of the PMSM Drives model and execute the MMPC algorithm. The collective parameters of the system are shown in Table II. The sampling time is 50μs.

TABLE II
System Parameters

Parameter	Symbol	Value	Unit
Number of pole pairs	PP	4	
Rated speed	ω_{ref}	1500	rpm
Stator inductor	L_s	2.53e-3	H
DC side voltage	V_{dc}	500	V
Permanent magnet flux linkage	Ψ_f	0.2	Wb
Stator resistance	R_s	1.29	Ω
Coefficient of inertia	J	0.00194	kg·m^2
Rated output power	P_{out}	1500	W
Rated torque	T_{em}	10	Nm

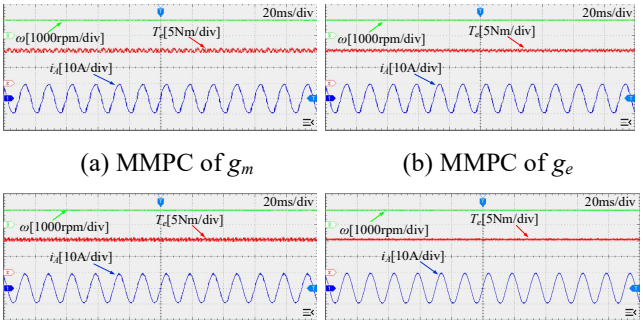

(a) MMPC of g_m (b) MMPC of g_e

(c) MMPC of g_{es} (d) Proposed scheme

Fig. 8. Response at 1000 rpm, 10 Nm load under steady-state condition.

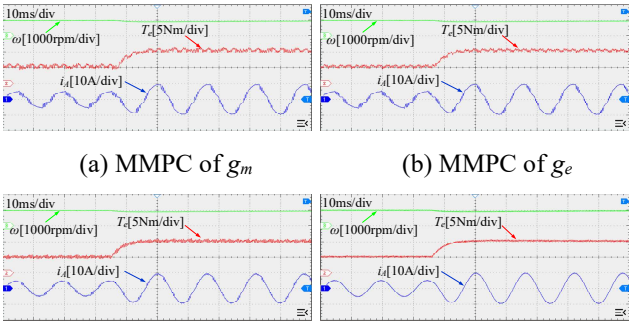

(a) MMPC of g_m (b) MMPC of g_e

(c) MMPC of g_{es} (d) Proposed scheme

Fig. 9. Dynamic deceleration for load variation from 5 Nm to 10 Nm.

B. Steady state performance

In order to test the steady-state performance of the proposed method, the torque, speed, and A-phase current waveforms of the four methods are shown in Fig. 8 when the speed is 1000rpm. The comparison results show that the torque ripple of this method is significantly lower than that of the other three methods. In addition, the proposed method significantly reduces the current THD due to the accuracy of the method in calculating the vector duty cycle. This result is completely consistent with the above theoretical explanation.

C. Dynamic state performance

To evaluate the dynamic performance of the proposed method, the waveform was measured under sudden changes in load torque from 5 Nm to 10 Nm. The dynamic responses of the three methods are shown in Fig. 9. It can be seen that because the four methods have the same outer loop speed loop controller, they all have faster velocity responses. However, compared with the other three methods, the waveform under the proposed method is smoother.

V. Experimental Results

A. Rig set-up

In order to further validate the effectiveness of the algorithm proposed, physical experiments are carried out in this section. The YanxuSP2000−based PMSM control drive platform is built, as shown in Fig. 10. The parameters are consistent with the hardware-in-the-loop test. The sampling frequency in the experiment is set to 10 kHz. Experimental data are collected and stored by the host computer and oscilloscope and imported into MATLAB for analysis.

B. Steady state performance

In order to verify the performance of the control algorithm, the motor is tested at different running speeds. Fig. 11 shows

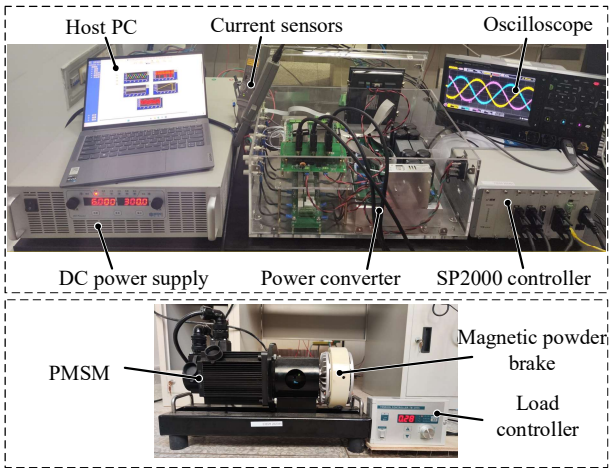

Fig. 10. Experimental platform.

the drive performance of the motor at a speed of 500 rpm. In addition, steady-state performance at 800 rpm and 1000 rpm is shown in Fig. 12 and Fig. 13. The response shown in Figs 11-13 includes the speed, torque, and current waveforms. The current is measured and recorded by an oscilloscope, and the speed and torque are recorded by the upper computer.

It can be clearly observed from Figs. 11-13 that the four methods show similar trends under different working points. That is, the proposed method has significantly lower speed ripple and torque ripple than the other three MMPC methods. At the same time, the three-phase current generated by the proposed method is smoother and less harmonic. This is mainly due to the accuracy of duty cycle calculation. The experimental results are consistent with the theoretical analysis and HIL results mentioned above.

C. Dynamic state performance

The dynamic response of the system is further studied, and the effectiveness of the proposed control technique is verified. In order to achieve this, the experiments of the motor inversion and sudden load increase are carried out respectively. Speed deceleration from 500rpm to -500rpm is shown in Fig. 14. Similarly, when the load torque step, the response is shown in Fig. 15. From these responses, it can be seen that the proposed method has the similar dynamic performance to the traditional MMPC schemes and has the advantage of improving the

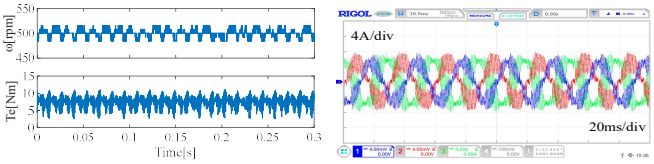

(a) MMPC of g_m

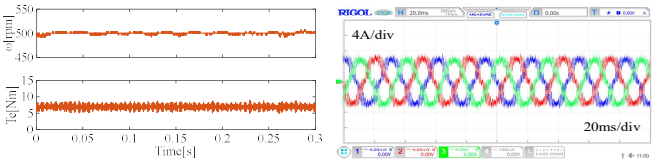

(b) MMPC of g_e

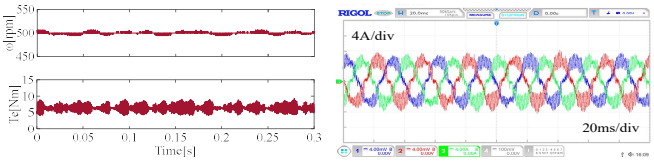

(c) MMPC of g_{es}

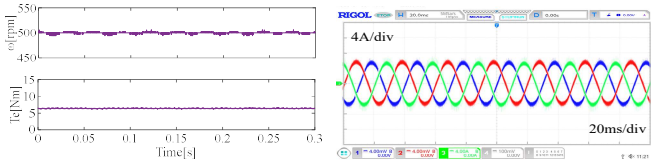

(d) Proposed scheme

Fig. 11. Response at 500 rpm under steady-state condition.

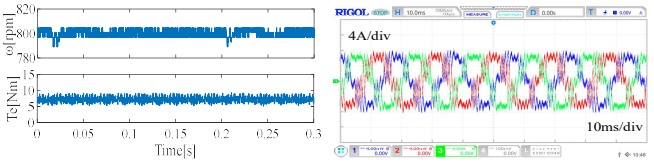

(a) MMPC of g_m

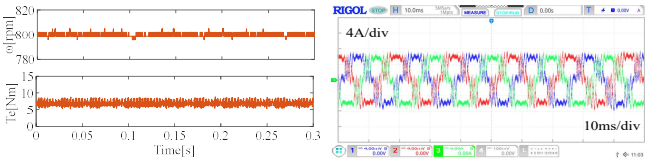

(b) MMPC of g_e

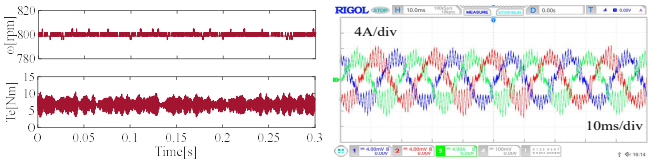

(c) MMPC of g_{es}

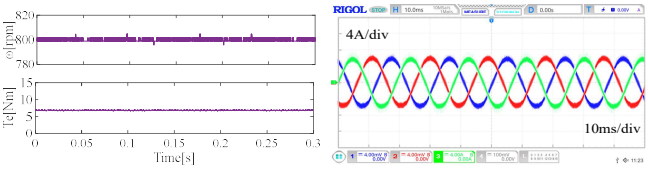

(d) Proposed scheme

Fig. 12. Response at 800 rpm under steady-state condition.

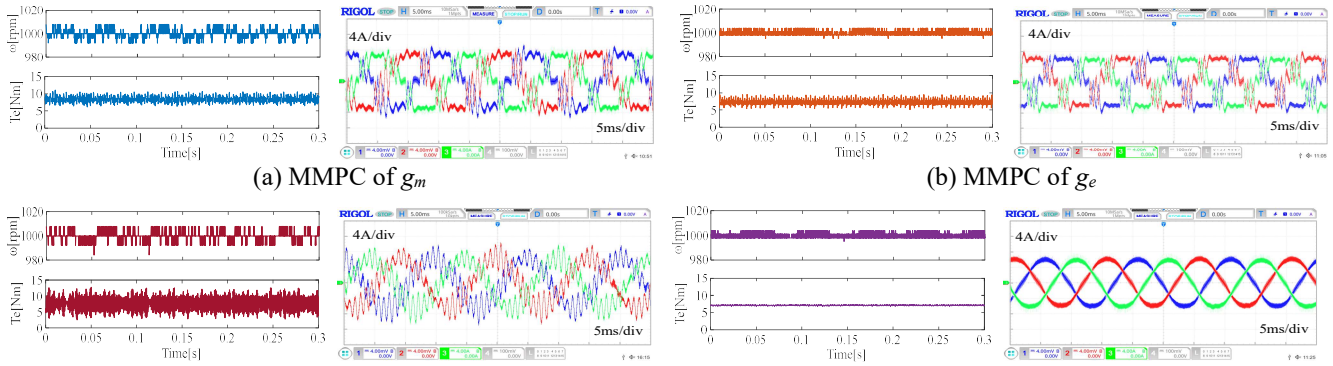

(a) MMPC of g_m (b) MMPC of g_e

(c) MMPC of g_{es} (d) Proposed scheme

Fig. 13. Response at 1000 rpm under steady-state condition.

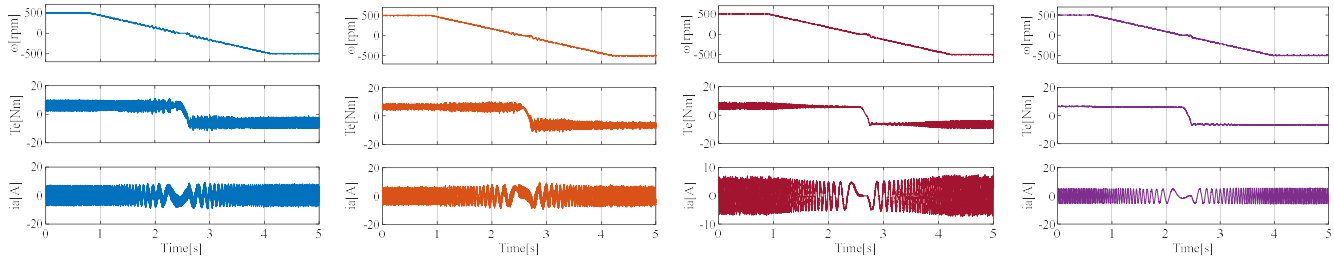

(a) MMPC of g_m (b) MMPC of g_e (c) MMPC of g_{es} (d) Proposed scheme

Fig. 14. Dynamic deceleration for speed variation from 500 rpm to -500 rpm.

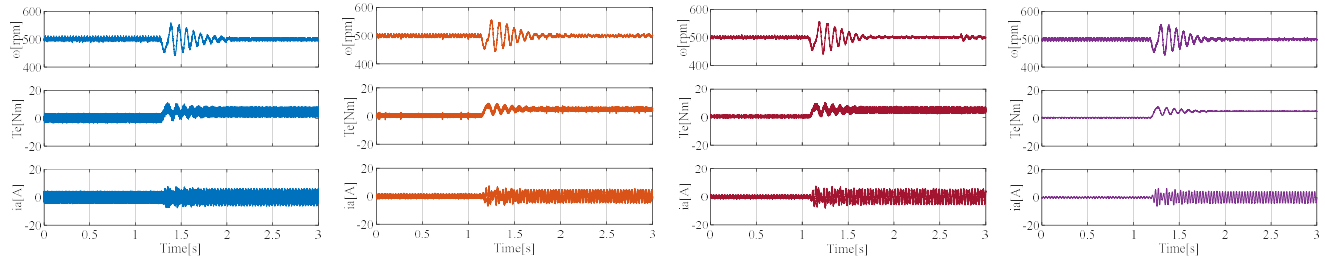

(a) MMPC of g_m (b) MMPC of g_e (c) MMPC of g_{es} (d) Proposed scheme

Fig. 15. Dynamic torque variation.

steady-state performance. The duty cycle is calculated by vector projection without any CF and optimization steps; thus, the proposed method does not increase the computational complexity of the algorithm.

D. Results Discussion

In this section, the representative MMPC methods are compared and summarized in Table III. The classical PI controller with space vector pulse width modulation (SVPWM) technique is also included in the comparison. The evaluation criteria include computational burden, duty cycle calculation, whether trigonometric functions are required, dynamic performance, design complexity, and steady-state performance.

In terms of computational burden, the classical PI-SVPWM control method has the worst effect in terms of computation because the volt-second balance in the modulation stage requires trigonometric operation. MMPC method [21], [24] and MMPC method [27] and [28], which use dead-beat and virtual vector technology to calculate duty cycle and select vectors through traversal, will also increase the calculation burden. In contrast, the proposed method uses vector projection to calculate duty cycle and vector selection, and its computational burden is similar to that of the traditional MMPC method. The dynamic performance is mainly affected by the amount of computation, and the smaller the amount of computation, the superior the dynamic response.

In terms of design complexity, the traditional PI-SVPWM control method needs to design proportional integral parameters, which is relatively complicated. Other methods do not need to carry out this step, and the design complexity is relatively low. The steady-state performance of the system mainly depends on the accuracy of duty cycle calculation, thus the improved MMPC method, PI-SVPWM, and the proposed method are superior to the traditional MMPC in steady-state performance.

TABLE III

EVALUATION OF REPRESENTATIVE MOTOR CONTROL METHODS WITH THE PROPOSED TECHNIQUE

Control Methods	PI-SVPWM in [5]	Traditional MMPC	MMPC in [21] [24]	MMPC in [27] [28]	**Proposed MMPC**
Computational Burden	✗ ✗	√ √	✗	√	**√ √**
DC calculation	volt-second balance principle	CF	dead-beat	virtual vector	vector projection
Involve trigonometric functions	Yes	No	No	No	**No**
Dynamic Performance	✗ ✗	√ √	✗	√	**√ √**
Design Complexity	✗ ✗	√ √	√	√	**√**
Steady-state Performance	√ √	✗	√ √	√	**√ √**

Scaled from best (√√) to worst (✗ ✗)

VI. CONCLUSIONS

Through a visual analysis approach, this paper vividly illustrates the inaccuracy of traditional MMPC methods in duty cycle calculation. Building upon this, a novel CF-free-based MMPC strategy utilizing vector projection is proposed. Compared with the traditional MMPC method, the main contribution of this proposed approach is the significant improvement in the system's steady-state performance without increasing computational complexity. This is achieved by utilizing constructed WF and geometric relationships, and accurately calculating vector duty cycle through basic arithmetic operations. The effectiveness of this method is demonstrated by visual analysis. Also, the superiority of this method is verified by the hardware-in-the-loop test and experiment of the control system of PMSM under various working conditions.

REFERENCES

[1] T. Wu *et al.*, "Enhanced Model Predictive Control for PMSM Based on Reference Voltage Predictive Model," *IEEE J. Emerg. Sel. Topics Power Electron.*, vol. 11, no. 5, pp. 5290–5300, Oct. 2023.

[2] Z. Huang, Q. Wei, R. Zhu, and Y. Xia, "Improved Modulated Model Predictive Control Technique for PMSM Drives Using the Vector Projection," *IEEJ Transactions Elec Engng*, p. tee.23994, Jan. 2024.

[3] Z. Chen and J. Qiu, "Adjacent-Vector-Based Model Predictive Control for Permanent Magnet Synchronous Motors With Full Model Estimation," *IEEE J. Emerg. Sel. Topics Power Electron.*, vol. 11, no. 2, pp. 1317–1331, Apr. 2023.

[4] I. G. Prieto, M. J. Duran, P. Garcia-Entrambasaguas, and M. Bermudez, "Field-Oriented Control of Multiphase Drives With Passive Fault Tolerance," *IEEE Trans. Ind. Electron.*, vol. 67, no. 9, pp. 7228–7238, Sep. 2020.

[5] H. Hadla and F. Santos, "Performance Comparison of Field-oriented Control, Direct Torque Control, and Model-predictive Control for SynRMs," *Chin. J. Electr. Eng.*, vol. 8, no. 1, pp. 24–37, Mar. 2022.

[6] J. Rodriguez *et al.*, "Latest Advances of Model Predictive Control in Electrical Drives—Part I: Basic Concepts and Advanced Strategies," *IEEE Trans. Power Electron.*, vol. 37, no. 4, pp. 3927–3942, Apr. 2022.

[7] J. Rodriguez *et al.*, "Latest Advances of Model Predictive Control in Electrical Drives—Part II: Applications and Benchmarking With Classical Control Methods," *IEEE Trans. Power Electron.*, vol. 37, no. 5, pp. 5047–5061, May 2022.

[8] I. Harbi *et al.*, "Model Predictive Control of Multilevel Inverters: Challenges, Recent Advances, and Trends," *IEEE Trans. Power Electron.*, pp. 1–24, 2023.

[9] B. Zhang *et al.*, "A Novel Simplified Finite Control Set Repeat Model Predictive Control for Grid-Connected Inverters," *IEEE Trans. Ind. Electron.*, vol. 70, no. 11, pp. 11324–11333, Nov. 2023.

[10] Changliang Xia, Tao Liu, Tingna Shi, and Zhanfeng Song, "A Simplified Finite-Control-Set Model-Predictive Control for Power Converters," *IEEE Trans. Ind. Inf.*, vol. 10, no. 2, pp. 991–1002, May 2014.

[11] H. Lin, S. Niu, Z. Xue, and S. Wang, "A Simplified Virtual-Vector-Based Model Predictive Control Technique With a Control Factor for Three-Phase SPMSM Drives," *IEEE Trans. Power Electron.*, vol. 38, no. 6, pp. 7546–7557, Jun. 2023.

[12] S.-W. Kang, J.-H. Soh, and R.-Y. Kim, "Symmetrical Three-Vector-Based Model Predictive Control With Deadbeat Solution for IPMSM in Rotating Reference Frame," *IEEE Trans. Ind. Electron.*, vol. 67, no. 1, pp. 159–168, Jan. 2020.

[13] L. Guo, M. Chen, Y. Li, P. Wang, N. Jin, and J. Wu, "Hybrid Multi-Vector Modulated Model Predictive Control Strategy for Voltage Source Inverters Based on a New Visualization Analysis Method," *IEEE Trans. Transp. Electrific.*, vol. 9, no. 1, pp. 8–21, Mar. 2023.

[14] S. Yan, Y. Cui, and C. Li, "Modulated FCS-MPC Based on Zero-Sequence Component Injection Algorithm and Vector Synthesis Algorithm With NPP Deviation Suppression," *IEEE Trans. Ind. Electron.*, pp. 1–12, 2023.

[15] F. Yu, K. Li, Z. Zhu, and X. Liu, "An Over-Modulated Model Predictive Current Control for Permanent Magnet Synchronous Motors," *IEEE Access*, vol. 10, pp. 40391–40401, 2022.

[16] M. L. Parvathy and V. K. Thippiripati, "A Simplified Voltage Vector Preselection-Based Multivector Predictive Current Control for Improved Torque Performance of PMSM Drive," *IEEE Trans. Power Electron.*, vol. 38, no. 7, pp. 8775–8785, Jul. 2023.

[17] F. Donoso, A. Mora, R. Cardenas, A. Angulo, D. Saez, and M. Rivera, "Finite-Set Model-Predictive Control Strategies for a 3L-NPC Inverter Operating With Fixed Switching Frequency," *IEEE Trans. Ind. Electron.*, vol. 65, no. 5, pp. 3954–3965, May 2018.

[18] Y. Yang *et al.*, "Multiple-Voltage-Vector Model Predictive Control With Reduced Complexity for Multilevel Inverters," *IEEE Trans. Transp. Electrific.*, vol. 6, no. 1, pp. 105–117, Mar. 2020.

[19] L. Tarisciotti, P. Zanchetta, A. Watson, J. C. Clare, M. Degano, and S. Bifaretti, "Modulated Model Predictive Control for a Three-Phase Active Rectifier," *IEEE Trans. on Ind. Applicat.*, vol. 51, no. 2, pp. 1610–1620, Mar. 2015.

[20] L. Tarisciotti *et al.*, "Model Predictive Control for Shunt Active Filters With Fixed Switching Frequency," *IEEE Trans. on Ind. Applicat.*, vol. 53, no. 1, pp. 296–304, Jan. 2017.

[21] D. Xiao, K. S. Alam, M. Norambuena, M. F. Rahman, and J. Rodriguez, "Modified Modulated Model Predictive Control Strategy for a Grid-Connected Converter," *IEEE Trans. Ind. Electron.*, vol. 68, no. 1, pp. 575–585, Jan. 2021.

[22] Y. Yang, H. Wen, and D. Li, "A Fast and Fixed Switching Frequency Model Predictive Control With Delay Compensation for Three-Phase Inverters," *IEEE Access*, vol. 5, pp. 17904–17913, 2017.

[23] L. Guo, N. Jin, Y. Li, and K. Luo, "A Model Predictive Control Method for Grid-Connected Power Converters Without AC Voltage Sensors," *IEEE Trans. Ind. Electron.*, vol. 68, no. 2, pp. 1299–1310, Feb. 2021.

[24] O. Gonzalez *et al.*, "Model Predictive Current Control of Six-Phase Induction Motor Drives Using Virtual Vectors and Space Vector

Modulation," *IEEE Trans. Power Electron.*, vol. 37, no. 7, pp. 7617–7628, Jul. 2022.

[25] Z. Gong, J. Li, P. Dai, D. Su, and X. Wu, "Design and Evaluation of a Virtual Vector Based Modulated Model Predictive Control for the Indirect Matrix Converters With Improved Performance," *IEEE Trans. Ind. Electron.*, vol. 69, no. 12, pp. 12019–12029, Dec. 2022.

[26] M. Ayala, J. Doval-Gandoy, O. Gonzalez, J. Rodas, R. Gregor, and M. Rivera, "Experimental Stability Study of Modulated Model Predictive Current Controllers Applied to Six-Phase Induction Motor Drives," *IEEE Trans. Power Electron.*, vol. 36, no. 11, pp. 13275–13284, Nov. 2021.

[27] Q. Xiao *et al.*, "Dual-Layer Modulated Model Predictive Control Scheme for the Cascaded H-Bridge Converter," *IEEE Trans. Ind. Electron.*, vol. 70, no. 10, pp. 9751–9763, Oct. 2023.

[28] Y. Li and H. Zhu, "Three-Vector Model Predictive Suspension Force Control for Bearingless Permanent Magnet Slice Motor," *IEEE Trans. Power Electron.*, vol. 38, no. 7, pp. 8282–8290, Jul. 2023.